Enhanced faint companion photometry and astrometry using wavelength diversity

Daniel Burke* and Nicholas Devaney

School of Physics, National University of Ireland Galway, Galway, Ireland
**Corresponding author: daniel.burke@nuigalway.ie*

Received April 13, 2010; revised July 29, 2010; accepted August 3, 2010;
posted August 18, 2010 (Doc. ID 126412); published September 28, 2010

In this paper we examine approaches to faint companion detection and estimation in multi-spectral images. We will employ the Hotelling observer, which is the optimal linear algorithm for signal detection. We have shown how to use this observer to estimate faint object position and brightness in the presence of residual speckle, which usually limits astrometric and photometric techniques. These speckles can be reduced by differential imaging techniques such as Angular Differential Imaging and Spectral Differential Imaging. Here we present results based on simulations of adaptive-optics-corrected images from an Extremely Large Telescope (ELT) that contain quasi-static speckle noise. The simulation includes Angular Differential Imaging and Spectral Differential Imaging to reduce the residual speckle and subsequent multi-wavelength processing. We examine the feasibility of this approach on simulated ELT observations of faint companions. © 2010 Optical Society of America

OCIS codes: 010.1080, 030.6140, 100.2960, 100.4993, 100.5070, 350.1270.

1. INTRODUCTION

The direct imaging of faint companions in high-contrast adaptive optics images is limited by quasi-static speckles present in the point-spread function (PSF) of the parent star [1]. Our approach to overcoming this limit combines PSF estimation from multi-wavelength data with the use of a prewhitening matched filter, referred to as the Hotelling observer, to perform the differential photometry and astrometry. This approach is combined with classical differential imaging to reduce the effects of speckle noise. We concentrate on cases where the faint companion ($\Delta m = 10$) is located well within the bright halo of the parent star.

The Hotelling observer is sometimes referred to as a prewhitening matched filter [2,3]. In the process of prewhitening, the data are divided by the data covariance matrix with the aim of producing spatially stationary, uncorrelated noise. The data covariance model requires a good PSF estimate; the PSF estimate is used to subtract the signal of the bright star from the image (PSF subtraction), flatten the residuals (prewhitening), and estimate the companion signal via matched filtering.

Our current study is based on simulations of adaptive-optics-corrected images from the European Extremely Large Telescope (E-ELT) with added quasi-static speckle noise. The simulated data were created using the end-to-end AO simulation package PAOLA [4]. The simulation includes Angular Differential Imaging (ADI) [5] and Spectral Differential Imaging (SDI) [6]. The simulation takes into account the strong methane absorption feature of giant planets and brown dwarfs modeled by Marley *et al.* [7], where there is a large change in the flux of a companion from 1.4 μm up to 2 μm. The data were simulated at two wavelengths, $\lambda = 1.8$ μm and 1.64 μm. The companion is bright at 1.8 μm, $\Delta m_{1.8\ \mu\mathrm{m}} = 10$, and faint in the 1.64 μm data set, $\Delta m_{1.64\ \mu\mathrm{m}} = 15$.

In Section 2 we introduce the difficulties in calculating differential astrometry and photometry of faint companions in the presence of quasi-static speckles. Two differential techniques to reduce the level of speckle noise are also reviewed. In Section 3 our approach to PSF estimation from multi-wavelength data is presented. The Hotelling observer for computing astrometry and photometry is derived in Section 4 and our combined algorithm in Section 5. This is followed in Section 6 with a comparison of the astrometric and photometric accuracy of the estimated PSF. The paper concludes in Section 7 with a discussion of the performance of the algorithm and some suggestions for future study.

2. QUASI-STATIC SPECKLE NOISE

Attempting to detect a faint companion above the bright halo produced by diffraction wings in stellar images is very difficult. When imaging with adaptive optics from the ground, the uncorrected part of the incoming wavefront will produce a random intensity fluctuation in this halo. This pattern is referred to as residual speckle. These residual speckles arise mainly from two sources: short-exposure "atmospheric" speckles pinned to the diffraction pattern of the telescope and quasi-static speckles from uncorrected aberrations in the system, e.g., imperfections in the adaptive optics (AO) optics [8]. These instrumentally induced quasi-static speckles [5] will not average out over time [8,9], but produce a time varying PSF.

In order to reduce this quasi-static speckle noise, Racine *et al.* [6] proposed to subtract images taken simultaneously at two different wavelengths. Two procedures are needed before the images are subtracted: [10]:

 © 2010 Optical Society of America

1. one of the frames must be rescaled, as the speckle pattern size is proportional to λ.
2. the bandpass filters must be close together to preserve the similarities in the speckle structure.

Using this method speckle noise attenuation on the order of a factor of ~2 has been reported [5]. Another differential technique is ADI [11], which is similar to the roll deconvolution technique, developed to reduce the effect of static aberrations in the Hubble Space Telescope.

This approach consists of acquiring a sequence of images with the telescope's instrument rotator turned off. The stability of the quasi-static PSF structure is improved while the field of view with respect to the instrument now slowly rotates over the course of the observation. The ADI approach reduces speckle noise in two steps:

1. removal of correlated speckles by subtraction of a reference PSF,
2. averaging of the residual noise by combining the residual images after the field of view is re-aligned by de-rotation.

The reference PSF is created from the acquired sequence of images by taking the mean of a number of images for which the faint companion has moved significantly, but the PSF has not changed. The level of noise reduction is a function of the angular separation of the companion and the parent star, the time interval between the image and its reference PSF, and the image exposure time. While imaging in this mode on Altair NIRI [12] at the Gemini telescope, a quasi-speckle noise attenuation of a factor of ~100 was reported while observing Vega.

3. PSF RECONSTRUCTION USING WAVELENGTH DIVERSITY

Phase diversity, or wavelength diversity in our study, refers to a method that can be used to infer phase aberrations from image data. This methods allows one to estimate both an unknown observed object and the unknown phase aberrations of an imaging system. This technique was first proposed by Gonsalves and Childlaw [13,14] and later refined by Paxman *et al.* [15]. The phase aberration parameters are estimated by minimizing an objective function, which requires at least two images of the object, but does not depend on the object estimate. Typically one of the detected images is a conventional focal-plane image that is degraded by unknown aberrations, such as those induced by atmospheric turbulence, misaligned optics, or imperfections in the mirrors of the telescope. The second image of the same object is formed by perturbing these unknown aberrations in some known fashion, e.g., adding a known amount of defocus or changing the observed wavelength [16,17]. The two recorded images can be expressed as

$$g_1(r) = f * h_1(r) + n_1(r),$$

$$g_2(r) = f * h_2(r) + n_2(r), \tag{1}$$

where $*$ stands for convolution, r is the vector of image locations, f is the "true object," h_1 and h_2 represent the two PSFs, and n_1, n_2 are additive noise in the imaging system. Gonsalves and Childlaw [13] proposed to estimate the phase aberrations through the minimization of an error metric that measures the sum of the square errors in the difference between the observed image and the reconstructed image. When the rms fluctuations are the same for all pixels in the two images this metric can be shown to be equivalent to the maximum-likelihood estimator for additive Gaussian noise. When the rms values σ_1 and σ_2 of the noise are not the same, the error metric can be written as

$$L = \sum_u \{|G_1(u) - F(u)H_1(u)|^2 + \gamma|G_2(u) - F(u)H_2(u)|^2\}, \tag{2}$$

where capital letters denote the Fourier transform of the corresponding lower case quantity, and u is the frequency vector in the Fourier domain. γ is given by

$$\gamma = \sigma_1^2/\sigma_2^2. \tag{3}$$

The optical transfer function H is directly related to the phase aberrations in the pupil [18]. The phase in the pupil can be approximated using an expansion of Zernike polynomials. The problem then reduces to estimating a vector α of Zernike coefficients that minimize Eq. (2).

The solution of the equation $\partial L/\partial F = 0$ gives an estimate of the object $\hat{F}$ that minimizes Eq. (2) for a fixed set of aberrations:

$$\hat{F} = \frac{G_1(u)H_1^*(u) + \gamma G_2(u)H_2^*(u)}{|H_1(u)|^2 + \gamma|H_2(u)|^2}, \tag{4}$$

where $*$ denotes complex conjugate. Substituting Eq. (4) into Eq. (2) results in an error metric that is dependent only on α:

$$L_m(\alpha) = \sum_u \frac{|G_1(u)H_2(u,\alpha) - G_2(u)H_1(u,\alpha)|^2}{|H_1(u,\alpha)|^2 + \gamma|H_2(u,\alpha)|^2}. \tag{5}$$

The vector of Zernike coefficients is then computed as

$$\hat{\alpha} = \arg\max_\alpha[-L_m(\alpha)]. \tag{6}$$

In our study the minimization of $L_m(\alpha)$ was carried out through a non-linear bounded minimization within the Matlab data analysis environment.

4. HOTELLING OBSERVER

The Hotelling observer is sometimes referred to as a prewhitening matched filter [2,3]. In the process of prewhitening, the data are divided by the data covariance matrix with the goal of producing spatially stationary, uncorrelated noise. In this article we use an estimated PSF from our wavelength diversity algorithm to obtain an estimate of the data covariance matrix. The Hotelling observer performs three operations on the data. The input to the observer is a processed image, i.e., dark-subtracted and flat-fielded; see Fig. 1(a). The first operation is to use the estimated PSF to subtract the signal of the bright central star from the image [see Fig. 1(b)]. The residual image is prewhitened, thereby flattening the residuals [see Fig.

1(c)]. Finally, an estimate of the companion signal is computed via a matched filter (see Fig. 1(d)). In the example presented in Fig. 1 the images are 100×100 pixels, the images are shown on a log scale, and the observer was supplied with the PSF used to create the data; hence a companion 10 magnitudes fainter than the primary was easily detected and located.

The task that we are concerned with is the estimation of the location and intensity of a faint companion in an AO-corrected image. For a given data set g, we can model the data under two hypotheses: $H_{1,r_{pl}}$, companion present at the position r_{pl}; and H_0, companion absent with the expressions:

$$H_0: g = \bar{g}_0 + n, H_{1,r_{pl}} = \underbrace{\bar{g}_0 + s_{r_{pl}}}_{\bar{g}_{1,r_{pl}}} + n, \tag{7}$$

where $\bar{g}_0$ denotes the mean image when the companion is absent, n is the noise assumed to be composed of Gaussian noise from the detector and Poisson noise from detection of the incident light, and $\bar{g}_{1,r_{pl}}$ is the mean image when the companion is present at r_{pl} with the true signal of the companion given by $s_{r_{pl}}=\bar{g}_{1,r_{pl}}-\bar{g}_0$.

The mean noisy images can be modeled as:

$$\bar{g}_0 = \underbrace{A_* h(r_*)}_{\text{star image}} + \underbrace{b}_{\text{background}}, \quad \bar{g}_{1,r_{pl}} = \underbrace{A_* h(r_*)}_{\text{star image}} + \underbrace{A_{pl} h(r_{pl})}_{\text{companion image}} + \underbrace{b}_{\text{background}}, \tag{8}$$

where A_* is the intensity of the bright star located at r_*, A_{pl} is the intensity of the companion located at r_{pl}, $h(r)$ is the PSF located at r, and b is the background intensity. Under the Gaussian noise assumption the two densities of g can be expressed as [19,20]

$$pr(g|H_0) = \left[\frac{1}{(2\pi)^M det(K_g)}\right]^{1/2} \times exp\left[-\frac{1}{2}(g-\bar{g}_0)^T K_g^{-1}(g-\bar{g}_0)\right],$$

$$pr(g|H_{1,r_{pl}}) = \left[\frac{1}{(2\pi)^M det(K_g)}\right]^{1/2} \times exp\left[-\frac{1}{2}(g-\bar{g}_0-s_{r_{pl}})^T K_g^{-1}(g-\bar{g}_0-s_{r_{pl}})\right]. \tag{9}$$

Here *det* denotes the determinant of a given matrix, superscript ^{T} denotes transpose, $pr(g|H)$ is the conditional probability density function of the data under the hypothesis H, either H_0 or $H_{1,r_{pl}}$, and K_g is the covariance matrix of the data, of size $M\times M$.

With the assumption of uncorrelated noise, the data covariance matrix K_g is diagonal with elements given by

$$[K_g]_{m,m'} = [A_* h_m(r_*) + b_m + \sigma_m^2]\delta_{m,m'}, \tag{10}$$

where $\delta_{m,m'}$ is the Kronecker delta function, σ^2 is the variance of the detector readout noise, and m represents the pixel index.

The optimal discriminant function for the task of differential astrometry and photometry, referred to as the ideal observer, is the likelihood ratio [21]

$$\Lambda(g|r_{pl}) = \frac{pr(g|H_{1,r_{pl}})}{pr(g|H_0)}. \tag{11}$$

If the position of the companion r_{pl} is unknown then the ideal observer can be applied at a set of test locations R. This observer is at a maximum at the true position of the companion $r_{pl}\in R$. This ideal scanning observer takes the form

$$\Lambda(g) = \max_{r_{pl}\in R} \Lambda(g|r_{pl}) = \max_{r_{pl}\in R} \frac{pr(g|H_{1,r_{pl}})}{pr(g|H_0)}. \tag{12}$$

The estimation of r_{pl} is then computed as

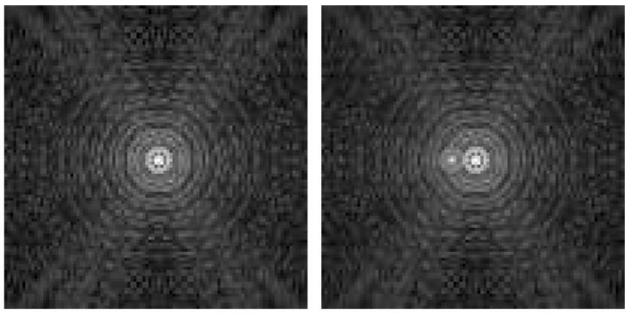

(a) Pre-processed Image (b) PSF Subtraction

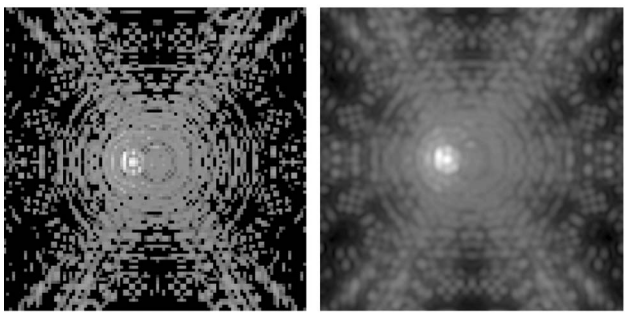

(c) Prewhitened (d) Matched Filtered

Fig. 1. Three operations of the Hotelling observer: (a) take a pre-processed image from which the signal of the central star is subtracted, (b) prewhiten the residual image, and (c) estimate the companion signal via a matched filter. (d) Note the companion signal is 10 magnitudes fainter than the parent star. All figures are shown on a log scale.

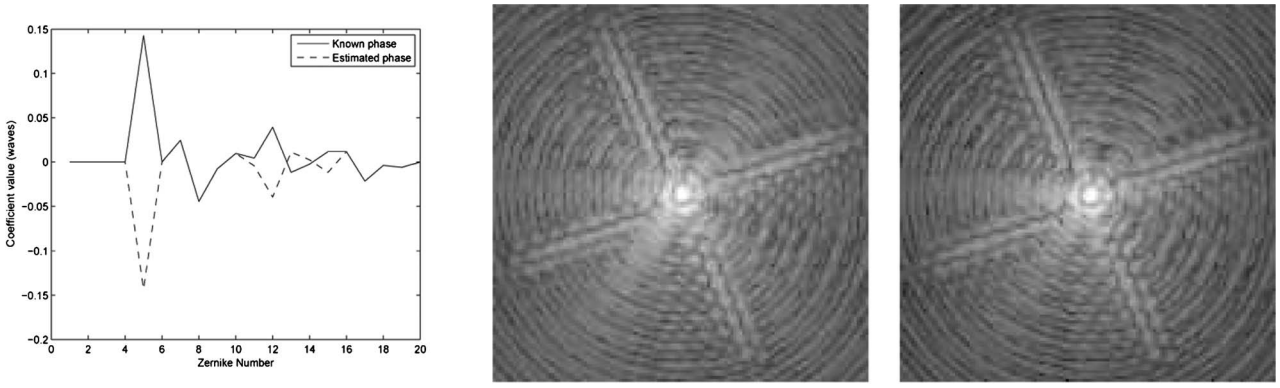

(a) Zernike Coefficient Estimates (b) PSF non-flipped Zernikes (c) PSF flipped Zernikes

Fig. 2. Initial simulations of our wavelength diversity approach resulted in pupil phase estimates with a sign ambiguity on the even radial order Zernike coefficients. The corresponding PSF estimates were identical due to the fact that if the pupil is symmetric, then the pupil autocorrelation of an even phase does not depend on the sign of that function.

$$\tilde{r}_{pl} = \arg\max_{r_{pl}\in R} \Lambda(g|r_{pl}). \tag{13}$$

Using the two Gaussian densities of the data and taking the logarithm of $\Lambda(g)$ we obtain the log-likelihood ratio $\lambda(g)=\ln[\Lambda(g)]$:

$$\lambda(g) = \max_{r_{pl}\in R}\left[s_{r_{pl}}^T K_g^{-1}\left(g - \bar{g}_0 - \frac{1}{2}s_{r_{pl}}\right)\right]. \tag{14}$$

The log-likelihood ratio $\lambda(g)$ being affine in g is the ideal linear observer. The Hotelling observer $t_{Hot}(g)$ is equal to $\lambda(g)$ if the data are normally distributed with equal covariances under both hypotheses. The scanning Hotelling observer takes on the form

$$t_{Hot}(g) = \max_{r_{pl}\in R}\sum_{m=1}^{M}\frac{A_{pl}h_m(r_{pl})}{A_* h_m(r_*) + b_m + \sigma_m^2}\left[g_m - \bar{g}_{0,m} - \frac{1}{2}A_{pl}h_m(r_{pl})\right]. \tag{15}$$

The estimation of the companion location r_{pl} is then computed as

$$\tilde{r}_{pl} = \arg\max_{r_{pl}\in R}[t_{hot}(g)]. \tag{16}$$

For every estimate of the location of the companion there exists an estimate of the intensity of the companion that maximizes the Hotelling test statistic for that location. Recalling the log-likelihood ratio, Eq. (14), the estimate of the companion's intensity A_{pl} for a defined set of test intensities A becomes

$$\tilde{A}_{pl} = \arg\max_{A_{pl}\in A}\left[s_{r_{pl}}^T K_g^{-1}(g - \bar{g}_0) - \frac{1}{2}s_{r_{pl}}^T K_g^{-1} s_{r_{pl}}\right]. \tag{17}$$

Equation (17) assumes r_{pl} is known. The log-likelihood ratio is maximized by taking the partial derivative with respect to A_{pl} and setting it equal to zero:

$$\frac{\partial t_{Hot}(g)}{\partial A_{pl}} = h(r_{pl})^T K_g^{-1}(g - \bar{g}_0) - A_{pl}h(r_{pl})^T K_g^{-1}h_m(r_{pl}) = 0, \tag{18}$$

where we made use of the fact that $s_{r_{pl}}=A_{pl}h(r_{pl})$. This leads to the following estimator for A_{pl}:

$$\tilde{A}_{pl} = \frac{h(r_{pl})^T K_g^{-1}(g - \bar{g}_0)}{h(r_{pl})^T K_g^{-1}h(r_{pl})}. \tag{19}$$

Recalling the structure of the data covariance matrix K_g we get

$$\tilde{A}_{pl} = \sum_{m=1}^{M}\frac{(h_m(r_{pl})/(A_* h_m(r_*) + b_m + \sigma_m^2))[g_m - \bar{g}_{0,m}]}{h_m(r_{pl})^2/(A_* h_m(r_*) + b_m + \sigma_m^2)}. \tag{20}$$

The estimation of the companion location is computed using Eq. (14) while substituting the estimation of A_{pl} from Eq. (20) into Eq. (14) for each test location. The result is astrometry and photometry of an observed companion.

5. SIMULATIONS

An initial test of our wavelength diversity phase retrieval algorithm was carried out by applying a known random phase to a simulated 8.1 m class telescope. A first guess at the vector of Zernike coefficients $\alpha_{initial}$ was computed as a vector of zero mean Gaussian random numbers scaled to follow a f^{-2} power law. Bounds were placed on the maximum and minimum values of the estimates of the Zernike coefficients, and the phase in the pupil plane was bounded by a binary pupil mask. In this test the algorithm was given 27 random starts, where the PSF with the minimum least square error between the estimated PSF and the data was taken as the best estimate. This result is shown in Fig. 2. As can be seen in Fig. 2(a) the Paxman least squares error metric [Eq. (5)] appears to be insensitive to the sign on the even radial order Zernike coefficients. This error on the sign of the even radial order Zernike coefficients is to be expected, since the PSF may

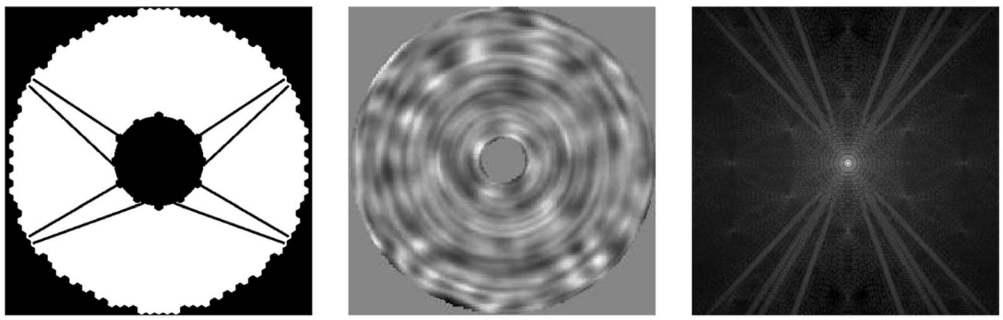

(a) Simulated E-ELT Pupil (b) VLT Error Map (c) Simulated E-ELT PSF (log scale)

Fig. 3. Simulating speckle noise on an ELT with PAOLA. The pupil of the E-ELT was modeled as a 42 m segmented primary mirror, (a). Static speckle noise was added to the pupil by using a scaled version of the VLT error map, (b). The resulting long exposure PSF, (c), is the combination of 30 short-exposure PSFs.

be obtained by Fourier transforming the autocorrelation function of the complex amplitude in the pupil; if the pupil is symmetric, then the pupil autocorrelation of an even phase function does not depend on the sign of that function. This can be verified using the fact that the autocorrelation of the pupil complex amplitude $a(u)$ and the autocorrelation of $a^*(-u)$ are equal. In this test we use a symmetric pupil function; in reality, it is probable that asymmetries in the pupil will remove this sign ambiguity.

In order to test our combined differential imaging and PSF estimation approach for the task of quasi-static speckle noise reduction and the estimation of the position and intensity of a faint companion in an AO-corrected image we used an end-to-end IDL (Interactive Data Language)-based package called PAOLA [4] (Performance of Adaptive Optics for Large/Little Apertures) to simulate a PSF based on the proposed E-ELT [22]. This method is based on modeling of the AO-corrected residual phase spatial power spectrum from which a good approximation of the long-exposure optical transfer function (OTF) can be calculated. There was no noise simulated in this AO system. The E-ELT simulation had the following parameters:

- 50 nm rms static aberrations on the primary mirror segments.
- 30 nm rms static aberrations within the instrument.
- 100 actuators across the 42 m diameter of the pupil.
- 10×1 second exposures.
- PSFs simulated at $\lambda = 1.64$ μm and 1.8 μm.
- Seeing ($\lambda = 0.5$ μm) $= 0.7''$.

The telescope was modeled having a 42 m primary segmented mirror with a 12.5 m central obscuration and four spider arms; see Fig. 3(a). Ten PSFs were generated at $\lambda = 1.64$ μm and another ten PSFs at $\lambda = 1.8$ μm that included static and quasi-static speckle noise. To include the effects of static speckle noise, we added to each simulated phase a static element—the error map of the Very Large Telescope [23] primary mirror [9,24]; see Fig. 3(b). This map was scaled to have the rms phase variation required, 50 nm, and scaled to have the same size as the 42 m pupil. For each 1 s exposure, a quasi-static noise-corrupted PSF was produced by co-adding the PSFs from 30 independent random realizations of the estimated residual phase spatial power spectral density generated by PAOLA. An example of the PSFs used is presented in Fig. 3(c).

Using the ten dual-wavelength PSF pairs an ADI type data set was simulated. In each image a faint companion was inserted into the scene with a separation of 0.0442 arcsec and a differential magnitude of $\Delta m_{1.8\ \mu\mathrm{m}} = 10$ and $\Delta m_{1.64\ \mu\mathrm{m}} = 15$. A field of view rotation of 18° from frame to frame in the image sequence was simulated such that the companion signal would not overlap in successive image frames. In practice such a field of view rotation can be achieved either by imaging close to the zenith, i.e., ≈30° [25] or by sampling the object at observing times

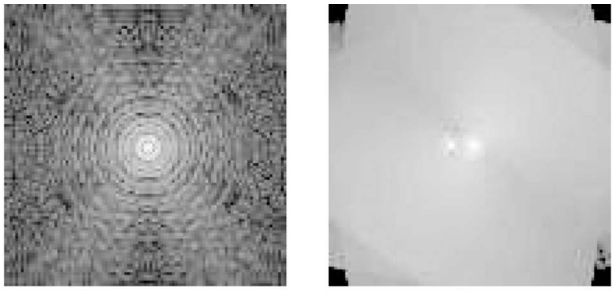

(a) Core of Estimated E-ELT PSF, from Wavelength Diversity (log scale) (b) ADI reduced image sequence (log scale)

(c) Core of Estimated E-ELT PSF, from mean of image sequence (log scale)

Fig. 4. PSF estimates were made using a wavelength diversity, (a), and by taking the mean of the ADI image sequence, (c). Subtracting the mean of the wavelength diversity PSF estimates from the data, derotating, and co-adding the residuals reveals the presence of the faint companion.

that are spaced sufficiently. The latter would have the drawback of covering different seeing conditions.

For each wavelength pair and rotation angle, wavelength diversity was used to estimate the phase in the pupil plane of the telescope. A PSF estimate was then obtained by Fourier propagating this phase to the image plane see; Fig. 4(a). The ten estimated PSFs, one for each wavelength channel, were averaged and the result subtracted from the corresponding data sequence. Each data sequence was subsequently derotated using bilinear interpolation, co-added, and the final images at the two wavelengths subtracted; see Fig. 4(b).

6. RESULTS

The ADI reduced image sequence was processed with the Hotelling observer, Eqs. (16) and (20), using the mean of the estimated PSFs; see Fig. 5. The maximum value of the Hotelling data map corresponded to the location and differential magnitude of the faint companion. As a PSF comparison the average of the image sequence was used to process the ADI reduced image under the assumption that the faint companion signal will be washed out in the averaging process; see Fig. 4(c). The Hotelling algorithm obtained the most accurate estimate for the position and intensity of the companion when using the wavelength-diverse PSF estimate; see Table 1. The improvement in differential photometry was on the order of 2.5% when compared to the photometry extracted using the mean of the image sequence as the PSF estimate. Comparably the error in differential astrometry dropped by 2% when using the wavelength-diverse PSF estimate over the mean of image sequence as the PSF estimate. These results support the conclusion that our wavelength-diversity method reconstructs an accurate estimate of the AO-corrected PSF.

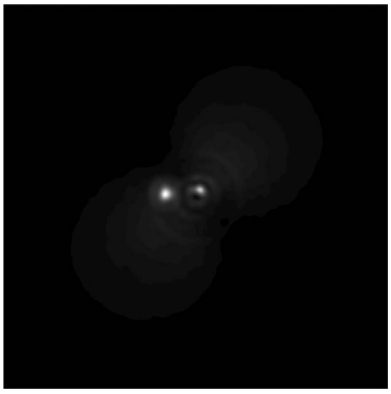

Fig. 5. Values of the Hotelling test statistic [Eq. (15)] for the ADI–SDI reduced image sequence; the maximum of this map corresponds to the position and intensity of the faint companion.

Table 1. Comparative Photometry and Astrometry Estimation Test

PSF	Error in Position Estimation	Error in Differential Magnitude
Average PSF from Wavelength Diversity	0.0028 arcsec	0.8 magnitudes
Mean of Image Sequence	0.0035 arcsec	1.05 magnitudes

7. CONCLUSION

We have presented a combined approach to reducing quasi-static speckle noise in highly corrected AO images from an ELT. Our method combines classical Angular Differential Imaging and Spectral Differential Imaging with PSF reconstruction from multi-wavelength data that is then used by the Hotelling observer to extract differential astrometry and photometry of a faint companion present in the quasi-static speckle halo.

The Hotelling algorithm was used to test the fidelity of the estimated PSF. The mean of the set of reconstructed PSFs produced a smaller error in the differential astrometry and photometry computed with the Hotelling observer compared with the mean of the image sequence. In the future we plan to compare this PSF estimation approach to more sophisticated methods such as the ADI-LOCI (Locally Optimized Combination of Images) [26] PSF reconstruction technique.

While the algorithm developed in this paper uses the information from only two wavelengths to reconstruct the phase in the pupil plane, we have found that this approach provides better results than simply averaging the image sequence to produce a PSF estimate. In this study the minimization process required approximately 1 hour per PSF pair, executed in Matlab on a 2.16 GHz Intel Core 2 Duo with 2 GB of RAM. The minimization function was not supplied with any derivative information and therefore had to use finite differences to approximate the gradient. The extension of the algorithm to three and possibly n wavelengths could lead to a more accurate estimate of the wavelength-independent pupil phase if a model of the change in the companion flux with wavelength were included. Such data would be available from an Integral Field Unit, and most exoplanet imagers will include this capability This in turn would produce a better data covariance matrix and hence more accurate estimation of the faint companion's position and intensity via the Hotelling observer.

ACKNOWLEDGMENTS

This research was funded by Science Foundation IrelandGrant No. 07/*IN*.1/*I*906. The authors wish to acknowledge the SFI/HEA Irish Centre for High-End Computing (ICHEC) for the provision of computational facilities and support.

REFERENCES

1. C. Aime and R. Soummer, "The usefulness and limits of coronagraphy in the presence of pinned speckles," Astrophys. J. **612**, L85–L88 (2004).
2. H. H. Barrett, K. J. Myers, M. N. Devaney, and J. C. Dainty, "Objective assessment of image quality. IV. Application to adaptive optics," J. Opt. Soc. Am. A **23**, 3080–3105 (2006).
3. D. Burke, S. Gladysz, L. Roberts, N. Devaney, and C. Dainty, "An improved technique for the photometry and as-

trometry of faint companions," Publ. Astron. Soc. Pac. **121**, 767–777 (2009).
4. L. Jolissaint, J. Véran, and R. Conan, "Analytical modeling of adaptive optics: foundations of the phase spatial power spectrum approach," J. Opt. Soc. Am. A **23**,382–394 (2006).
5. C. Marois, R. Doyon, D. Nadeau, R. Racine, M. Riopel, P. Vallee, and D. Lafreniere, "TRIDENT: an infrared differential imaging camera optimized for the detection of methanated substellar companions," Publ. Astron. Soc. Pac. **117**, 745–756 (2005).
6. R. Racine, G. A. H. A. H. Walker, D. Nadeau, R. Doyon, and C. Marois, "Speckle noise and the detection of faint companions," Publ. Astron. Soc. Pac. **111**, 587–594 (1999).
7. M. S. Marley, D. Saumon, T. Guillot, S. Freedman, W. B. Hubbard, A. Burrows, and J. I. Lunine, "Atmospheric, evolutionary, and spectral models of the brown dwarf gliese 229 B," Science **272**, 1919–1921 (1996).
8. S. Hinkley, B. R. Oppenheimer, R. Soummer, A. Sivaramakrishnan, L. C. Roberts, Jr., J. Kuhn, R. B. Makidon, M. D. Perrin, J. P. Lloyd, K. Kratter, and D. Brenner, "Temporal evolution of coronagraphic dynamic range and constraints on companions to Vega," Astrophys. J. **654**, 633–640 (2007).
9. S. Gladysz and J. C. Christou, "Detection of faint companions through stochastic speckle discrimination," Astrophys. J. **698**, 28–44 (2009).
10. C. Marois, R. Doyon, R. Racine, and D. Nadeau, "Efficient speckle noise attenuation in faint companion imaging," Publ. Astron. Soc. Pac. **112**, 91–96 (2000).
11. C. Marois, D. Lafreniere, R. Doyon, B. Macintosh, and D. Nadeau, "Angular differential imaging: A powerful high-contrast imaging technique," Astrophys. J. **641**, 556–564 (2006).
12. K. W. Hodapp, J. B. Jensen, E. M. Irwin, Y. H., R. Chung, K. Flectcher, L. Robertson, J. L. Hora, D. A. Simons, W. Mays, R. Nolad, M. Bec, M. Merrill, and A. M. Fowler, "The Gemini near-infrared imager (NIRI)," Publ. Astron. Soc. Pac. **115**, 1388–1406 (2003).
13. R. A. Gonsalves and R. Childlaw, "Wavefront sensing by phase retrieval," Proc. SPIE **207**, 32–39 (1979).
14. R. A. Gonsalves, "Phase retrieval and diversity in adaptive optics," Opt. Eng. (1982).
15. R. G. Paxman, T. J. Schulz, and J. R. Fienup, "Joint estimation of object and aberrations by using phase diversity," J. Opt. Soc. Am. A **9**, 1072–1085 (1992).
16. H. R. Ingleby and D. R. McGaughey, "Real data results with wavelength-diverse blind deconvolution," Opt. Lett. **30**, 489–491 (2005).
17. M. G. Löfdahl, T. E. Berger, and H. Seldin, "Two dual-wavelength sequences of high-resolution solar photospheric images captured over several hours and restored by use of phase diversity," Astron. Astrophys. **377**, 1128–1135 (2001).
18. J. M. Bonet, *Motions in the Solar Atmosphere* (ASSL Series, 1999).
19. C. W. Helstrom, "*Statistical Theory of Signal Detection*" (Pergamon, 1968).
20. L. Caucci, H. H. Barrett, N. Devaney, and J. J. Rodríguez, "Application of the Hotelling and ideal observers to detection and localization of exoplanets," J. Opt. Soc. Am. A **24**, B13–B24 (2007).
21. H. H. Barrett and K. Myres, "*Foundations of Image Science*" (Wiley Series in Pure and Applied Optics, 2004).
22. R. Gilmozzi and J. Spyromilio, "The European extremely large telescope," The Messenger **127**, 11–19 (2007).
23. "http://www.eso.org/projects/vlt/,".
24. "http://www.eso.org/vlt/unit-tel/m1unit. html/,".
25. E. Artigau, B. A. Biller, Z. Wahhaj, M. Hartung, L. M. Close, M. R. Chun, M. C. Liu, T. G., F. Rigaut, D. W. Toomey, and C. Ftaclas, "Nici: combining coronagraphy, adi, and sdi," Proc. SPIE **7014**, 70141–70149 (2008).
26. D. Lafrenière, C. Marois, R. Doyon, D. Nadeau, and E. Artigau, "A new algorithm for point-spread function subtraction in high-contrast imaging: a demonstration with angular differential imaging," Astrophys. J. **660**, 770–780 (2007).